Evidence for Scattering Resonances in the $H + D_2$ Reaction**

Félix Fernández-Alonso, Brian D. Bean, James D. Ayers, Andrew E. Pomerantz, Richard N. Zare,* Luis Bañares, and F. J. Aoiz

The concept of scattering resonances in chemical reactions was extensively discussed[1, 2] in the early 1970s to explain oscillations in the reaction probability calculated for collinear encounters of H with H_2. Since then, the nature of resonance behavior and its observation in this prototypical reaction system have been a topic of intense and sometimes heated interest. Scattering resonances were first introduced to explain sharp features in the collision cross-section of neutrons with heavy nuclei as a function of collision energy[3] and then in the elastic scattering of electrons in atoms.[4] These (Feshbach) resonances are associated with a quasibound complex formed by the collision partners. Thus, it is common to associate the width of the resonance with the lifetime of the compound system, and the location of the resonance with the energy of the quasibound state. This semiclassical picture was the basis for the explanation that Levine and Wu[2] gave to the collinear $H + H_2$ system. Subsequently, theory was extended to three dimensions[5] and resonance features were shown to persist, but to be less pronounced.

Experimental observation of resonance behavior in the hydrogen exchange reaction has lagged behind theoretical efforts. In the late 1980s, Nieh and Valentini[6] reported scattering resonances in the integral cross-section (ICS) for the $H + H_2$ reaction. Subsequent theoretical[7] and experimental[8] work, however, showed that resonances are not observable in the ICS, but should be detectable in the energy dependence of the state-resolved differential cross-section (DCS)[9, 10] for the $H + H_2$ and $D + H_2$ reactions. The past ten years have witnessed considerable progress on the experimental front with the first fully state-resolved DCS measurements in the $H + D_2$ reaction by Schnieder and co-workers[11, 12] and by Zare and co-workers.[13–15] Aided by the theoretical predictions of Wu and Kuppermann,[16] Wrede and Schnieder[17] attempted to observe resonances in the $H + D_2$ reaction by tuning the collision energy between 1.27 and 1.30 eV, but their experimental data did not show any resonance structure, which caused them to question the theory. Recently, Shafer-Ray and co-workers[18] have found experimental and theoretical evidence for resonance signatures in the integral cross-section for $H + D_2 \rightarrow HD(v' = 0, j' = 7) + D$ at 0.94 eV, while they are absent in its isotopic cousins $H + H_2$ and $D + H_2$.

Herein we report signatures of resonances in the state-resolved DCS for the $H + D_2 \rightarrow HD(v' = 3, j') + D$ reaction at a center-of-mass (CM) collision energy of 1.64 ± 0.05 eV (158 ± 5 kJ mol^{-1}). We also complement these measurements with simulations of the experimental results using the quasiclassical trajectory (QCT) method. Experimentally we find sharp forward scattering for the lowest j' rotational levels of the $HD(v' = 3)$ product, which we attribute to the formation of short-lived reaction intermediates, the classical analogue of quantum mechanical scattering resonances. To the best of our knowledge resonances have not been previously reported in the state-resolved differential cross-sections for any chemical reaction system.

Figure 1 shows a comparison between the experimental results and QCT calculations for the $HD(v' = 3, j' = 0-7)$ ICS. The error bars in both theory and experiment represent 1σ (67%) confidence bands. The QCT calculations incorporate an initial D_2 rotational distribution characterized by a

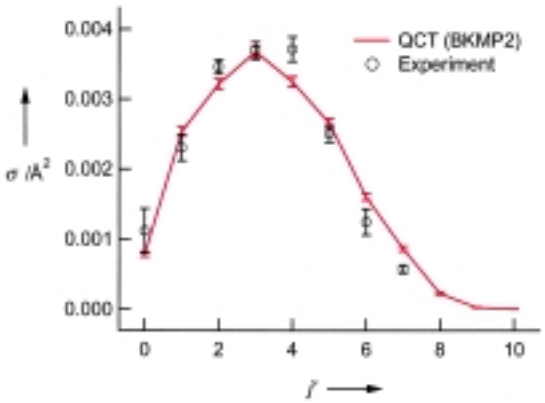

Figure 1. Reactive cross-section σ as a function of the $HD(v' = 3)$ product rotational state j'. The ordinate scale shown is for quasiclassical trajectory calculations (QCT, shown in red). The experimental points (open circles) have been normalized to the same total area as the QCT curve.

temperature of 300 K. The experimental technique employed in this study is sensitive only to the relative populations in different rotational levels. The experimental cross-sections have been scaled such that they have the same cumulative area from $j' = 0$ to 7 as the QCT calculations. No further scaling of the ICS or DCSs has been performed in the remainder of this work. Note the small reaction probabilities leading to the $HD(v' = 3, j')$ product. The scale on this plot ($0.000 - 0.004$ Å^2) should be compared with the total cross-section of 1.253 ± 0.001 Å^2 for the reaction obtained from the QCT calculations. The agreement between experiment and

[*] Prof. R. N. Zare, Dr. F. Fernández-Alonso, B. D. Bean, J. D. Ayers, A. E. Pomerantz
Department of Chemistry
Stanford University
Stanford, CA 94305-5080 (USA)
Fax: (+1) 650-725-0259
E-mail: zare@stanford.edu

Prof. L. Bañares, Prof. F. J. Aoiz
Departamento de Química Física
Facultad de Química
Universidad Complutense
28040 Madrid (Spain)

[**] We thank Donald G. Truhlar, Patrick Brown, Zee Hwan Kim, and Stephen Cho for careful and critical reading of the manuscript prior to publication. We also thank Andrew J. Alexander for his assistance in the preparation of the polar plots. Elf-Atochem (B.D.B.), the Hertz Foundation and Stanford University (J.D.A.), and the National Science Foundation (A.E.P.) are gratefully acknowledged for their support in the form of Graduate Fellowships. This work was supported at Stanford University by the U.S. National Science Foundation under Grant Number CHE-99-00305 and at Universidad Complutense by DGCYT PB98-0762-C03-01.

  1433-7851/00/3915-2748 $ 17.50+.50/0

theory at this level of detail is excellent. Small discrepancies might be removed when a full quantum mechanical scattering calculation is completed.[19]

Qualitatively, the shape of the rotational distribution is quite similar to what has been found for HD($v'=1,j'$) and HD($v'=2,j'$) at similar collision energies.[20] The highest rotational quantum number produced in this reaction is dictated by impact parameter constraints rather than energy conservation. (The impact parameter is defined as the distance of closest approach of the reagents in the absence of the interaction potential.) In a simple-minded model for this reaction the initial impact parameter for reaction is channeled into rotational excitation of the product, that is, glancing collisions are more likely to produce rotationally excited products than head-on collisions.

Apart from the measurement of the product yield in a particular quantum state, we have also measured the state-resolved DCS in the CM frame. A DCS provides information about the preferred direction of HD product scattering (v_{HD}) with respect to the velocity of the incoming hydrogen atom (v_H). Backward scattering corresponds to an angle of 180° between v_H and v_{HD} (the two vectors being antiparallel). The opposite case (parallel velocity vectors) corresponds to forward scattering. In Figure 2 we present polar plots of the

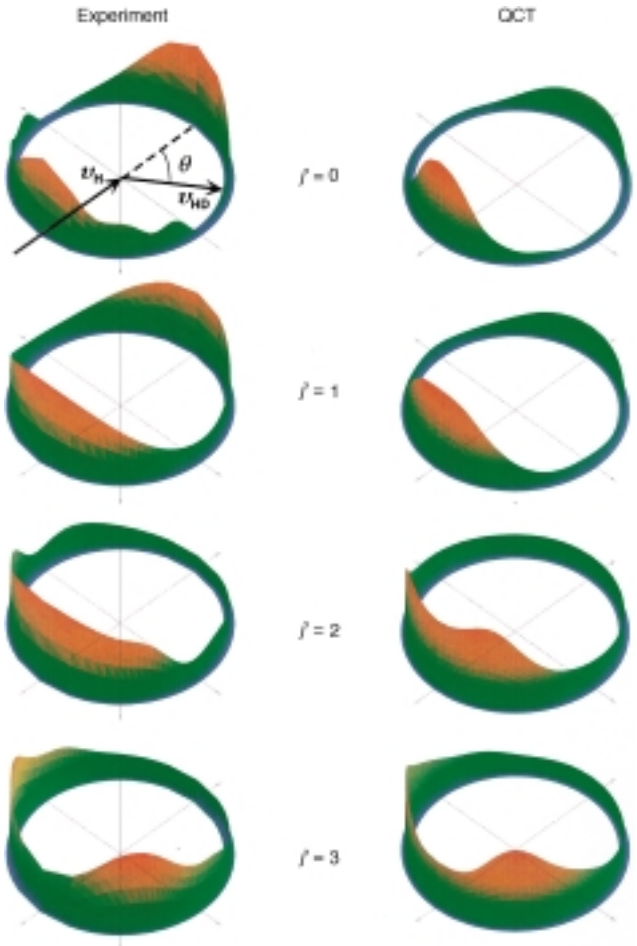

Figure 2. Polar plots of the HD($v'=3,j'=0-3$) CM differential cross-sections from experiment (left) and QCT calculations (right). The H atom reactant (v_H) and HD product (v_{HD}) CM velocities are indicated with arrows (see text for details).

experimental and QCT DCSs for HD($v'=3,j'=0-3$). In these plots the chemical reaction takes place in the plane of the figure, with the directions of v_H and v_{HD} defined as shown. The height around each circle is proportional to the probability of scattering into an angle θ, where θ is defined as the angle between v_H and v_{HD}.

The polar plots generated from the experimental data are shown on the left and have been obtained from a spline representation of a total of twelve experimental points across the whole angular range. The QCT DCSs shown on the right have been convolved with the instrumental function to provide the best simulation of the experimental results. In both cases, the DCSs show a similar dependence on j'. In the backward hemisphere ($\theta > 90°$) the DCSs move away from complete backward scattering as j' increases. This finding is also in qualitative agreement with previous findings for lower vibrational levels.[11, 13] The most striking feature in this figure is the peak in the forward direction which is most prominent for the rotationless state $j'=0$. The experimental and QCT polar plots in Figure 2 differ in regard to the ratio of forward to backward scattering. This finding suggests that the observations cannot be described solely by quasiclassical mechanics.

Despite the disagreement in the magnitude of the forward scattering peak between experiment and the QCT method, the fact that the calculations do actually show the same qualitative trends as the experiment caused us to examine the QCT reactive trajectories more closely. Figure 3 shows some of the attributes characterizing the reactive collisions that lead to HD($v'=3,j'=0-3$). The left panel shows the state-resolved reaction probabilities sorted in terms of those scattering in the forward ($\theta < 90°$) and backward hemispheres ($\theta > 90°$). The reaction cross-section is proportional to the integral of the reaction probability (opacity function) $P(b)$ × the impact parameter b. Therefore, the larger the impact parameter the larger the cross-section will be for a given value of $P(b)$. For backward scattering, the reaction probability shifts in b as the amount of product rotation increases. This trend is consistent with our previous interpretation of the shape and extent of the ICS (Figure 1). In contrast, the forward-scattering reaction probability peaks at 0.7–0.8 Å. This value for the impact parameter is close to the internuclear distance for molecular hydrogen and its isotopomers. Moreover, its shape and position seem not to depend strongly on the product rotational quantum number. This figure helps to explain why forward scattering has been observed primarily for low j' states. It is seen that the $j'=0$ back-scattered reaction probability peaks at lower b values than for $j'=1-3$. Very similar reaction probability distributions have been previously observed in QCT trajectory calculations of the $D+H_2$ reaction between 0.30 and 1.25 eV by Aoiz and co-workers.[21] The contribution of the high impact parameter to the DCS in the $D+H_2$ reaction was associated with the "E-θ ridge" which also appeared in the quantum mechanical calculations of Miller and Zhang and was associated with resonance scattering.[10] Prior to these studies, Muga and Levine[22] had proposed a classical mechanism for resonances in $H+H_2$ collisions that involved high impact parameters as well as long collision times. As shown below, we also find that our

  1433-7851/00/3915-2749 $ 17.50+.50/0

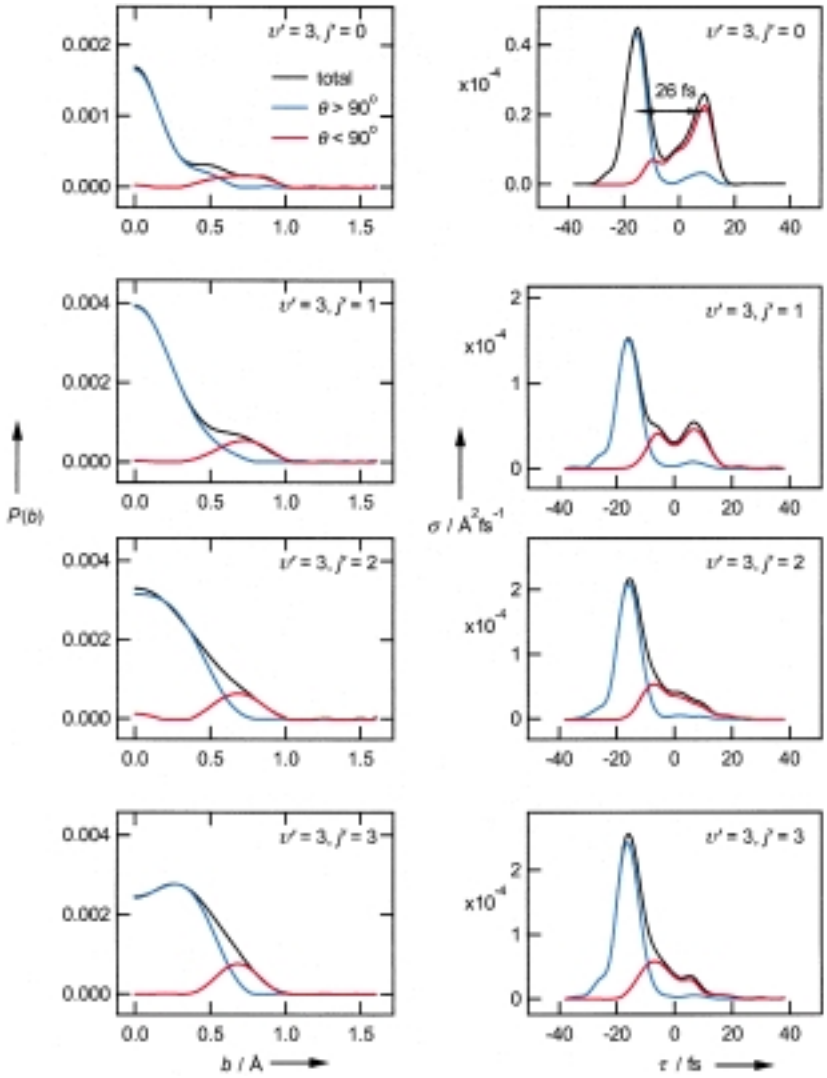

Figure 3. QCT trajectory details for HD($v'=3,j'=0-3$). The plots on the left show the reaction probability $P(b)$ as a function of impact parameter b for all, backward, and forward reactive trajectories. The plots on the right show the reactive cross-sections σ as a function of time delay τ for all, backward, and forward trajectories (see text for further details).

forward-scattering peak is associated with long-lived trajectories.

We also show the distribution of time delays (a measure of the reaction time) corresponding to the forward- and backward- scattering products that accompany the reaction probabilities in Figure 3. The classical time delay τ is defined as the time difference for trajectories with and without the potential present.[21–23] We observe negative time delays (typical for direct reactions) for the back-scattered classical trajectories, whereas the forward-scattering ones appear at more positive time delays. An approximate time difference of 26 fs between direct (backward) and indirect (forward) trajectories is calculated for the HD($v'=3,j'=0$) state (Figure 3). This time difference is considerably shorter than the classical period for the first rotational state of the HD product (120 fs) and HDD complex (480 fs). Therefore, the observed forward–backward scattering does not arise from a complex that lives for one or more rotational periods.

Distinct forward and backward contributions are most prominent for the HD($v'=3,j'=0$) product state. The peak at positive time delay has decreased considerably for the HD($v'=3,j'=1-3$) states relative to the backward (direct) contribution. Moreover, the forward-scattering time delay gradually decreases in going from $j'=0$ to $j'=3$. This finding further corroborates the conclusion that long-lived trajectories appear most prominently in the DCS for the HD($v'=3$, $j'=0$) product state.

It is possible to offer a tentative explanation for the resonance behavior based on our previous analysis of reactive trajectories and on the features of the potential energy surface. The top panel in Figure 4 shows two typical trajectories corresponding to the indirect/forward (left) and direct/backward (right) scattering mechanisms. The numbered dots indicate particular collision times for each trajectory (1 = earliest, 4 = latest). The inset defines the entrance-channel Jacobi coordinates R and γ used in this figure to plot the trajectories and potential energy contours. Here R is the distance between the H atom and the center of mass of the D_2 molecule, and γ is the angle between R and the D_2 bond axis. The middle and bottom panels show contours of the BKMP2[24] potential energy surface with the D_2 bond distance fixed at the equilibrium distance of 0.74 Å (middle) and at 1.21 Å (bottom). The trajectory dots corresponding to the elongation of each diatom bond are overlaid on these contours. The H atom approaches the diatom almost collinearly ($\gamma \approx 180^\circ$) in the direct, back-scattered trajectory. As a result, a minimum value of R is reached (dot 2 on the right) without the D_2 molecule adjusting its internuclear distance. Immediately after this "hard" knock, the D_2 bond breaks giving rise to vibrationally excited HD product (dot 3 on the right). The initial geometry of the three atoms for the indirect/forward trajectory tends to be L-shaped ($\gamma = 30-60^\circ$) and the angular variable γ changes rapidly as the H atom approaches the D_2 molecule. This deflection is mainly caused by the large barrier to insertion located at $\gamma \approx 90^\circ$ (see bottom contour plot). During this time, the D_2 molecule elongates its bond. By the time R approaches its minimum value, the topology of the potential energy surface displays two deep wells about the collinear configuration. The red dots 2–4 in the bottom panel appear to rattle around these minima for a few femtoseconds. Although this picture is only qualitatively correct, namely, the width and depth of the wells is continuously being modulated by the changing diatomic bond length, it shows what features of the underlying energy surface give rise to our observations. The presence of relatively long-lived trajectories that correlate with observed forward-scattering features is likely to give rise to quasibound states in full quantum-mechanical calculations for this reaction system, and will hopefully account for the quantitative differences between experiments and QCT

  1433-7851/00/3915-2750 $ 17.50+.50/0

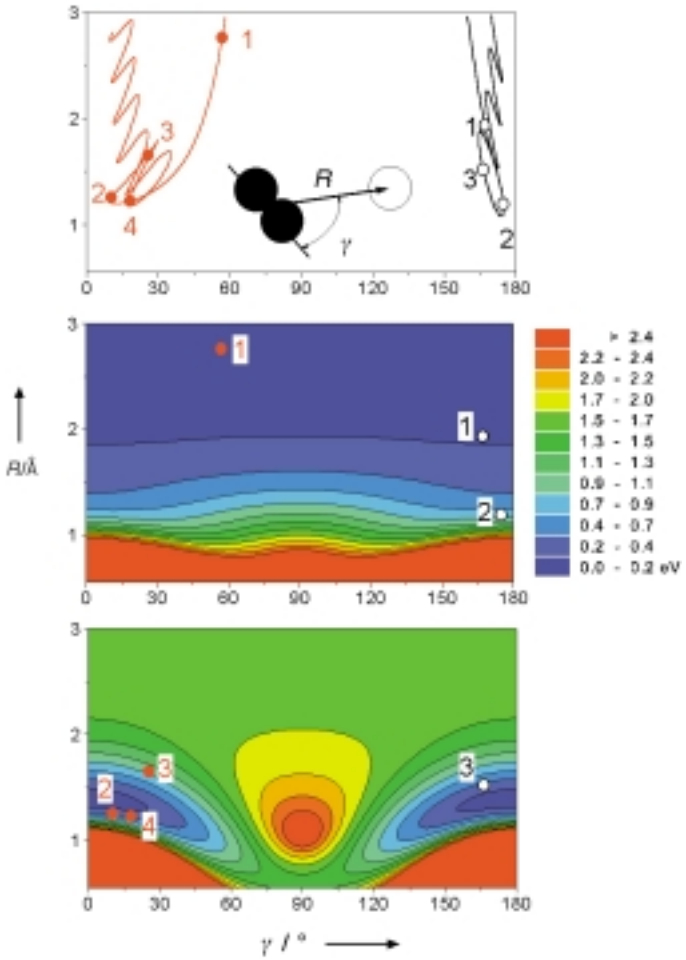

Figure 4. Top panel: R-γ plots of typical indirect (red line on the left) and direct (black line on the right) trajectories. Middle and bottom panels: potential energy contours of the BKMP2 potential energy surface with the D_2 bond length fixed at 0.74 Å (middle plot) and 1.21 Å (bottom). The trajectory dots have been overlaid on the potential energy contours corresponding to the instantaneous D_2 bond length. The color scale shown applies to both the middle and bottom contour plots.

calculations. Clearly resonance features provide detailed information on how this most elementary of chemical reactions can be understood.

Experimental Section

State-resolved DCS measurements: A mixture of HBr:D_2 (1:9) held at a stagnation pressure of 330 Torr was expanded into a high-vacuum chamber with a pulsed solenoid valve. HBr is photolyzed by the fifth harmonic of a Nd:YAG laser at 212.8 nm. Photolysis of this molecule generates two single-speed populations of "hot" hydrogen atoms. Only those hydrogen atoms corresponding to the fast photolysis channel contribute to our measured reaction signal. The HD($v'=3, j'=0-7$) reaction product is subsequently ionized 15 ns later by 2+1 resonance-enhanced multiphoton ionization (REMPI) through the $EF\,^1\Sigma_g^+ - X\,^1\Sigma_g^+$ electronic transition. Photolysis and reaction take place inside a velocity-sensitive, Wiley–McLaren time-of-flight apparatus. State-resolved CM DCSs can be directly inferred from an analysis of the time-of-flight profiles. Zare and co-workers have discussed in detail the experimental setup as well as the procedure to invert the experimental data into CM DCSs.[14]

QCT calculations: A total of five million trajectories were run on the BKMP2[24] potential energy surface at a relative translational energy of 1.64 eV. Each trajectory was initiated at a distance of 5 Å and numerically integrated in increments of 5.0×10^{-17} s using Hamming's fourth-order, predictor-corrector method. A trajectory was considered complete once the collision partners were also 5 Å apart. Asymptotic product analysis was performed at this final interparticle separation. Conservation of energy of 1 part in 10^5 and total angular momentum of 1 part in 10^6 in each trajectory was enforced throughout the calculation. No reactive trajectories were observed above 1.39 Å. Product quantization was performed by equating the internal energy of the HD product to the full Dunham expansion of rotational-vibrational levels and rounding these real values to the nearest integer.[25] The experimental rotational distribution of D_2 ($T=300$ K) was simulated by weighted sampling of the first nine rotational levels of this molecule. DCSs, reaction probabilities, and other reaction attributes were fit to a series in Legendre polynomials to provide a convenient functional representation of the computational results.[25, 26]

Received: March 31, 2000 [Z14928]

[1] a) D. G. Truhlar, A. Kuppermann, *J. Chem. Phys.* **1972**, *56*, 2232; b) G. C. Schatz, A. Kuppermann, *J. Chem. Phys.* **1973**, *59*, 964.
[2] R. D. Levine, S.-F. Wu, *Chem. Phys. Lett.* **1971**, *11*, 557.
[3] a) H. A. Bethe, *Phys. Rev.* **1935**, *47*, 747; b) N. Bohr, *Nature* **1936**, *137*, 344.
[4] a) E. Baranger, E. Gerjouy, *Phys. Rev.* **1957**, *106*, 1182; b) G. J. Schulz, *Phys. Rev. Lett.* **1962**, *10*, 104.
[5] G. C. Schatz, A. Kuppermann, *Phys. Rev. Lett.* **1975**, *35*, 1266.
[6] a) J. C. Nieh, J. J. Valentini, *Phys. Rev. Lett.* **1988**, *60*, 519; b) J. C. Nieh, J. J. Valentini, *J. Chem. Phys.* **1990**, *92*, 1083.
[7] a) M. Mladenovic, M. Zhao, D. G. Truhlar, D. W. Schwenke, Y. Sun, D. J. Kouri, *Chem. Phys. Lett.* **1988**, *146*, 358; b) J. Z. H. Zhang, W. H. Miller, *Chem. Phys. Lett.* **1988**, *153*, 465; c) D. E. Manolopoulos, R. E. Wyatt, *Chem. Phys. Lett.* **1989**, *159*, 123; d) J. Z. H. Zhang, W. H. Miller, *Chem. Phys. Lett.* **1989**, *159*, 130; e) M. Zhao, M. Mladenovic, D. G. Truhlar, D. W. Schwenke, *J. Am. Chem. Soc.* **1989**, *111*, 852; f) J. M. Launay, M. LeDourneuf, *Chem. Phys. Lett.* **1989**, *163*, 178.
[8] D. A. V. Kliner, D. E. Adelman, R. N. Zare, *J. Chem. Phys.* **1991**, *94*, 1069.
[9] R. E. Continetti, J. Z. H. Zhang, W. H. Miller, *J. Chem. Phys.* **1990**, *93*, 5356.
[10] W. H. Miller, J. Z. H. Zhang, *J. Phys. Chem.* **1991**, *95*, 12.
[11] a) L. Schnieder, K. Seekamp-Rahn, E. Wrede, K. H. Welge, *J. Chem. Phys.* **1997**, *107*, 6175; b) E. Wrede, L. Schnieder, K. H. Welge, F. J. Aoiz, L. Bañares, J. F. Castillo, B. Martínez-Haya, V. J. Herrero, *J. Chem. Phys.* **1999**, *110*, 9971.
[12] L. Schnieder, K. Seekamp-Rahn, J. Borkowski, E. Wrede, K. H. Welge, F. J. Aoiz, L. Bañares, M. J. D'Mello, V. J. Herrero, V. Sáez Rábanos, R. E. Wyatt, *Science* **1995**, *269*, 207.
[13] a) F. Fernández-Alonso, B. D. Bean, R. N. Zare, *J. Chem. Phys.* **1999**, *111*, 1035; b) F. Fernández-Alonso, B. D. Bean, R. N. Zare, *J. Chem. Phys.* **1999**, *111*, 2490.
[14] F. Fernández-Alonso, B. D. Bean, R. N. Zare, *J. Chem. Phys.* **1999**, *111*, 1022.
[15] H. Xu, N. E. Shafer-Ray, F. Merkt, D. J. Hughes, M. Springer, R. P. Tuckett, R. N. Zare, *J. Chem. Phys.* **1995**, *103*, 5157.
[16] A. Kuppermann, Y. S. M. Wu, *Chem. Phys. Lett.* **1995**, *241*, 229.
[17] E. Wrede, L. Schnieder, *J. Chem. Phys.* **1997**, *107*, 786.
[18] B. K. Kendrick, L. Jayasinghe, S. Moser, M. Auzinsh, N. Shafer-Ray, *Phys. Rev. Lett.* **2000**, *84*, 4325.
[19] J. F. Castillo, L. Bañares, F. J. Aoiz, unpublished results.
[20] B. D. Bean, F. Fernández-Alonso, R. N. Zare, *J. Phys. Chem.*, submitted.
[21] a) F. J. Aoiz, V. J. Herrero, V. S. Rábanos, *J. Chem. Phys.* **1991**, *95*, 7767; b) F. J. Aoiz, V. J. Herrero, V. S. Rábanos, *J. Chem. Phys.* **1992**, *97*, 7423.
[22] J. G. Muga, R. D. Levine, *Chem. Phys. Lett.* **1989**, *162*, 7.
[23] a) L. Eisenbud, PhD thesis, Princeton University (USA), **1948**; b) E. P. Wigner, *Phys. Rev.* **1955**, *98*, 145; c) F. T. Smith, *Phys. Rev.* **1960**, *118*, 349; d) J. W. Duff, D. G. Truhlar, *Chem. Phys.* **1974**, *4*, 1; e) P. Brumer, D. E. Fitz, D. Wardlaw, *J. Chem. Phys.* **1980**, *72*, 386;

f) A. Kuppermann in *Potential Energy Surfaces and Dynamics Calculations* (Ed.: D. G. Truhlar), Plenum, New York, **1981**, pp. 375.
[24] A. I. Boothroyd, W. J. Keogh, P. G. Martin, M. R. Peterson, *J. Chem. Phys.* **1996**, *104*, 7139.
[25] F. J. Aoiz, L. Bañares, V. J. Herrero in *Advances in Classical Trajectory Methods, Vol. 3* (Ed.: W. L. Hase), JAI, New York, **1998**, pp. 121.
[26] F. J. Aoiz, L. Bañares, V. J. Herrero, *J. Chem. Soc. Faraday Trans.* **1998**, *94*, 2483.

New Chiral Auxiliaries for the Construction of Quaternary Stereocenters by Copper-Catalyzed Michael Reactions**

Jens Christoffers* and Alexander Mann

The enantioselective construction of quaternary stereocenters is still a challenging goal in synthetic organic chemistry.[1] Herein we report a new copper(II)-catalyzed and auxiliary-based Michael reaction which allows the construction of quaternary carbon centers with *ee* values in excess of 95% at ambient temperature (see Scheme 1). The Michael reaction is an established method for C–C bond formation and is commonly catalyzed by a strong Brønstedt base.[2] In order to avoid the disadvantages of basic reaction conditions, a number of transition metal catalyzed procedures has been published in recent years; this has resulted in improved chemoselectivity due to the milder reaction conditions.[3] Moreover, chiral ligands can be utilized here to achieve asymmetric catalysis of the Michael reaction. In the recent years a number of chiral catalysts has been reported for the conversion of 1,3-dicarbonyl compounds with α,β-unsaturated ketones.[4] In particular, the introduction of the heterobimetallic lanthanum/sodium/[1,1′-binaphthyl]-2,2′-diol (LSB) catalyst by Shibasaki and co-workers has to be mentioned here as it defines the state of the art in this field.[5] However, the reaction conditions are also Brønstedt basic, and the enantioselective construction of quaternary stereocenters requires low temperatures.

Another strategy is the derivatization of the Michael donor with a chiral amine as an auxiliary to give an imine or enamine, which is subsequently converted with the Michael acceptor.[6] If enamines derived from β-oxoesters are applied according to this method, further activation, by addition of a stoichiometric amount of Lewis acid or by high pressure and low temperature, is required in order to achieve reasonable yields and selectivity.[7] Recently we reported on the Ni-catalyzed conversion of cyclic β-oxoesters in the presence of 1,2-diaminocyclohexane.[8] We were able to prepare the Michael product **6a** in 91% *ee* at ambient temperature and without exclusion of moisture. Similar results can only be achieved with the LSB catalyst at $-50\,^{\circ}C$ (93% *ee*).[9] Koga and co-workers obtained *ee* values of 90% by using a chiral auxiliary and a stoichiometric amount of a Brønstedt base at $-100\,^{\circ}C$.[10] In this work we report on a new class of auxiliaries for the transition metal catalyzed reaction of β-oxoesters **1** with simple enones, such as methyl vinyl ketone (MVK, **4**), and the synthesis of the Michael product **6a** (Scheme 1) with up to 99% *ee* at ambient temperature and without inert conditions, a reaction which is unprecedented in the literature.

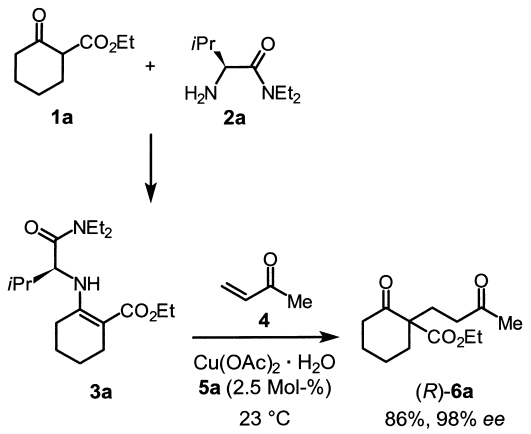

Scheme 1. Synthesis of **3a** and the copper(II)-catalyzed conversion with MVK (**4**).

In the course of a combinatorial search,[11] we have investigated a number of chiral amines **2a**–**p** derived from α-amino acids which bear either a thioether, a tertiary amine, or an amide group as an additional donor function.[12, 13] In an

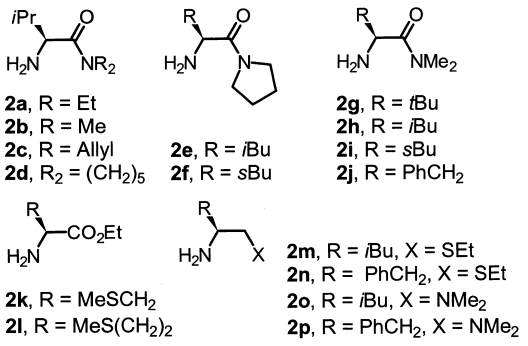

acid-catalyzed reaction with the Michael donor **1a**, these amines yield the corresponding imines, which exist completely as the tautomeric enamines **3a**–**p**; these enamines are isolable, after chromatography, in good to excellent yields (85–95%).

In a primary screening the enaminoesters **3a**–**p** were each converted in the presence of catalytic amounts of 14 different metal salts **5a**–**n**[14] with MVK (**4**) in CH_2Cl_2. If a positive effect was observed relative to the noncatalyzed reaction, with regard to the selectivity of the formation of Michael product **6a**, we started to optimize the reaction parameters. At this first stage of the screening, we did not pay attention to the

[*] Dr. J. Christoffers, Dipl.-Chem. A. Mann
Technische Universität Berlin
Institut für Organische Chemie, Sekretariat C3
Strasse des 17. Juni 135, 10623 Berlin (Germany)
Fax: (+49) 30-723-12-33
E-mail: jchr@wap0105.chem.tu-berlin.de

[**] This work was supported by the Deutsche Forschungsgemeinschaft and the Fonds der Chemischen Industrie. We are also grateful to the Degussa-Hüls AG for gifts of amino acids and to Prof. Dr. S. Blechert for his support.

  1433-7851/00/3915-2752 $ 17.50+.50/0